Article

Mutagenesis of Morphinone Reductase Induces Multiple Reactive Configurations and Identifies Potential Ambiguity in Kinetic Analysis of Enzyme Tunneling Mechanisms

Christopher R. Pudney, Sam Hay, Jiayun Pang, Claire Costello, David Leys, Michael J. Sutcliffe, and Nigel S. Scrutton

J. Am. Chem. Soc., **2007**, 129 (45), 13949-13956• DOI: 10.1021/ja074463h • Publication Date (Web): 16 October 2007

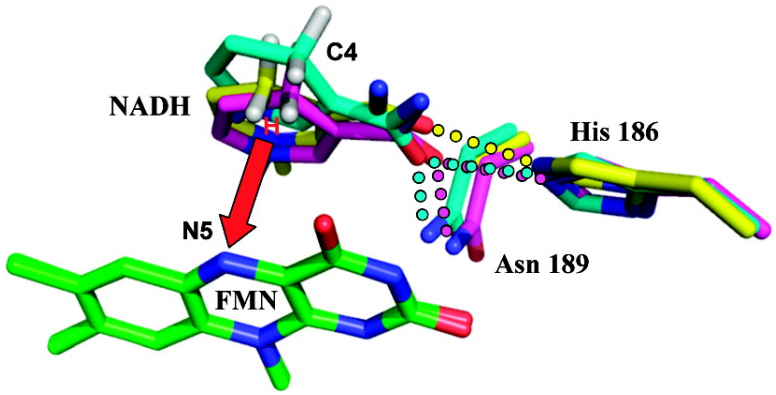

More About This Article

Additional resources and features associated with this article are available within the HTML version:

- Supporting Information
- Links to the 9 articles that cite this article, as of the time of this article download
- Access to high resolution figures
- Links to articles and content related to this article
- Copyright permission to reproduce figures and/or text from this article

View the Full Text HTML

J|A|C|S
ARTICLES
Published on Web 10/16/2007

Mutagenesis of Morphinone Reductase Induces Multiple Reactive Configurations and Identifies Potential Ambiguity in Kinetic Analysis of Enzyme Tunneling Mechanisms

Christopher R. Pudney,[†,‡] Sam Hay,[†,‡] Jiayun Pang,[†,§] Claire Costello,[†,‡] David Leys,[†,‡] Michael J. Sutcliffe,[†,§] and Nigel S. Scrutton*[,†,‡]

Contribution from the Manchester Interdisciplinary Biocentre, Faculty of Life Sciences, and School of Chemical Engineering and Analytical Science, University of Manchester, 131 Princess Street, Manchester, M1 7DN, U.K.

Received June 19, 2007; E-mail: nigel.scrutton@manchester.ac.uk

Abstract: We have identified multiple reactive configurations (MRCs) of an enzyme−coenzyme complex that have measurably different kinetic properties. In the complex formed between morphinone reductase (MR) and the NADH analogue 1,4,5,6-tetrahydro-NADH ($NADH_4$) the nicotinamide moiety is restrained close to the FMN isoalloxazine ring by hydrogen bonds from Asn-189 and His-186 as determined from the X-ray crystal structure. Molecular dynamic simulations indicate that removal of one of these hydrogen bonds in the N189A MR mutant allows the nicotinamide moiety to occupy a region of configurational space not accessible in wild-type enzyme. Using stopped-flow spectroscopy, we show that reduction of the FMN cofactor by NADH in N189A MR is multiphasic, identifying at least four different reactive configurations of the MR−NADH complex. This contrasts with wild-type MR in which hydride transfer occurs by environmentally coupled tunneling in a single kinetic phase [Pudney et al. *J. Am. Chem. Soc.* **2006**, *128*, 14053−14058]. Values for primary and α-secondary kinetic isotope effects, and their temperature dependence, for three of the kinetic phases in the N189A MR are consistent with hydride transfer by tunneling. Our analysis enables derivation of mechanistic information concerning different reactive configurations of the same enzyme−coenzyme complex using ensemble stopped-flow methods. Implications for the interpretation from kinetic data of tunneling mechanisms in enzymes are discussed.

Introduction

The ability to interpret macroscopic kinetic data in terms of the underpinning atomistic processes is a key factor in understanding the mechanism of enzyme action. Enzymes are kinetically complex systems, often requiring the extraction of microscopic rate constants from multiple turnover measurements.[1] A typical reaction cycle involves (i) substrate capture (binding), (ii) chemical transformation (reaction), and (iii) product release, each with their associated rate constants. Multiple turnover analysis has been augmented by isotope studies that have reported on chemical steps in the reaction cycle.[1,2] These include the use of competitive isotope effects[1,3−5] — and more recently studies of their temperature[5−7] and pressure[8−10] dependence — to report specifically on the chemical step(s). This approach has been exploited extensively in recent years to develop an understanding of enzymatic H-transfer and, in particular, to support full tunneling models for these reactions.[11−17]

A microscopic picture of key steps within enzyme catalytic cycles is beginning to emerge from atomistic simulations.[18,19] These suggest that the macroscopic rate constant comprises discrete rate constants arising from multiple reactant states and

[†] Manchester Interdisciplinary Biocentre.
[‡] Faculty of Life Sciences.
[§] School of Chemical Engineering and Analytical Science.

(1) Northrop, D. B. *Biochemistry* **1975**, *14*, 2644−2651.
(2) Swain, C. G.; Stivers, E. C.; Reuwer, J. F.; Schaad, L. J. *J. Am. Chem. Soc.* **1958**, *80*, 5885−5893.
(3) Cha, Y.; Murray, C. J.; Klinman, J. P. *Science* **1989**, *243*, 1325−1330.
(4) Wang, L.; Goodey, N. M.; Benkovic, S. J.; Kohen, A. *Proc. Natl. Acad. Sci. U.S.A.* **2006**, *103*, 15753−15758.
(5) Kohen, A.; Cannio, R.; Bartolucci, S.; Klinman, J. P. *Nature* **1999**, *399*, 496−499.
(6) Masgrau, L.; Roujeinikova, A.; Johannissen, L. O.; Hothi, P.; Basran, J.; Ranaghan, K. E.; Mulholland, A. J.; Sutcliffe, M. J.; Scrutton, N. S.; Leys, D. *Science* **2006**, *312*, 237−241.
(7) Pudney, C. R.; Hay, S.; Sutcliffe, M. J.; Scrutton, N. S. *J. Am. Chem. Soc.* **2006**, *128*, 14053−14058.
(8) Northrop, D. B. *J. Am. Chem. Soc.* **1999**, *121*, 3521−3524.
(9) Northrop, D. B.; Cho, Y. K. *Biochemistry* **2000**, *39*, 2406−2412.
(10) Hay, S.; Sutcliffe, M. J.; Scrutton, N. S. *Proc. Natl. Acad. U.S.A.* **2007**, *104*, 507−512.
(11) Knapp, M. J.; Rickert, K.; Klinman, J. P. *J. Am. Chem. Soc.* **2002**, *124*, 3865−3874.
(12) Kuznetsov, A. M.; Ulstrup, J. *Can. J. Chem.* **1999**, *77*, 1085−1096.
(13) Basran, J.; Sutcliffe, M. J.; Scrutton, N. S. *Biochemistry* **1999**, *38*, 3218−3222.
(14) Klinman, J. P. *Philos. Trans. R. Soc. London, Ser. B* **2006**, *361*, 1323−1331.
(15) Wang, L.; Goodey, N. M.; Benkovic, S. J.; Kohen, A. *Philos. Trans. R. Soc. London, Ser. B* **2006**, *361*, 1307−1315.
(16) Sutcliffe, M. J.; Masgrau, L.; Roujeinikova, A.; Johannissen, L. O.; Hothi, P.; Basran, J.; Ranaghan, K. E.; Mulholland, A. J.; Leys, D.; Scrutton, N. S. *Philos. Trans. R. Soc. London, Ser. B* **2006**, *361*, 1375−1386.
(17) Allemann, R. K.; Evans, R. M.; Tey, L. H.; Maglia, G.; Pang, J. Y.; Rodriguez, R.; Shrimpton, P. J.; Swanwick, R. S. *Philos. Trans. R. Soc. London, Ser. B* **2006**, *361*, 1317−1321.
(18) Ferrer, S.; Tunon, I.; Marti, S.; Moliner, V.; Garcia-Viloca, M.; Gonzalez-Lafont, A.; Lluch, J. M. *J. Am. Chem. Soc.* **2006**, *128*, 16851−16863.
(19) Thorpe, I. F.; Brooks, C. L. *J. Am. Chem. Soc.* **2005**, *127*, 12997−13006.

reaction paths.[18−20] This is supported by the stochastic nature of enzyme behavior observed in single molecule studies,[20−22] but our ability to detect these multiple states is generally beyond the scope of ensemble measurements of enzyme activity. This is compounded when the equilibrium of conformational states is perturbed by varying either temperature and/or pressure, tools commonly used, for example, to probe mechanisms of H-transfer in enzyme systems.[7,10,14−17]

Single turnover fast reaction measurements can give direct access to the chemical step of an enzyme catalyzed reaction, thus bypassing some of the limitations (e.g., kinetic complexity) associated with multiple turnover (steady-state) methods.[7,10,23,24] Single molecule approaches report on a single reaction configuration, whereas fast reaction methods are ensemble-based and typically provide an overall (single) microscopic rate constant for the ensemble of reactive species progressing through the chemical step. An alternative scenario is that in which different reactive states give rise to multiple, and kinetically detectable, microscopic rate constants corresponding to the chemical step.[18] This could occur when the configurations of the discrete reactive states are significantly different, for example, following mutagenesis of an enzyme active site (and even positions far from the active site) that leads to additional configuration(s) not accessible in the wild-type enzyme — a scenario described in this and other studies.[20,25] Such a situation would not be detected readily in multiple turnover (steady-state) studies. This is an important issue given current efforts to interpret steady-state data in terms of a mechanistic understanding of H-tunneling in enzyme systems.[3−5]

Single turnover studies in conjunction with single-molecule analysis of the FMN-containing enzyme dihydroorotate dehydrogenase (DHOD) have been used to identify multiple reactive configurations (MRCs) of a mutant enzyme−substrate complex.[20] Discrete rate constants for several reactive configurations in the reductive half-reaction were measured, although the authors were unable to extract mechanistic information from these data. Here we demonstrate how, in an enzyme system which has only one detectable reactive configuration, mutagenesis of the active site induces MRCs. With MRCs, the reaction occurs from each of the reactive configurations. This differs from "near attack conformers" (NACs),[26] which are ground state conformers that are geometrically similar to the transition state and which the reactant must pass through to enter the transition state; i.e., further configurational change occurs subsequent to passing through the NAC and prior to the reaction occurring. Using an ensemble fast reaction method we have detected a minimum of four discrete reactive configurations for the hydride transfer reaction from NADH to FMN in a mutant (Asn189 → Ala) form of the flavoprotein morphinone reductase (MR). By analyzing kinetic isotope effects, where a clear picture can be obtained, we show that hydride transfer occurs via an environmentally coupled H-tunneling mechanism. Our analysis highlights potential problems in using kinetic data derived from steady-state data for the analysis of H-tunneling in enzymes, especially with mutant forms, and emphasizes the need to perform (where possible) more direct analysis of the chemical step using single turnover fast reaction methods.

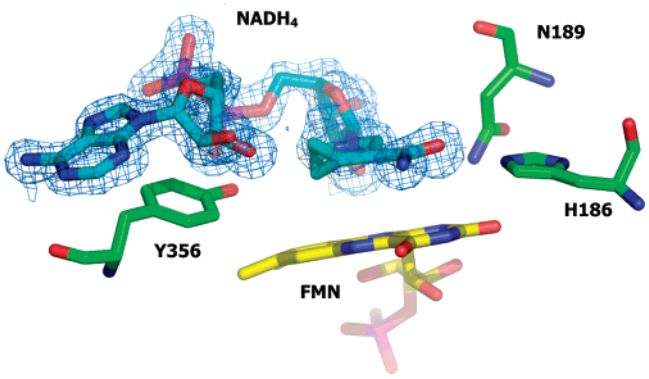

Figure 1. Active site of MR in complex with $NADH_4$. Key residues and both FMN and $NADH_4$ are shown in atom colored sticks, with carbons colored green for amino acids, yellow for the FMN and cyan for the $NADH_4$. The sigmaA weighted 2FoFc map surrounding the $NADH_4$ is contoured at 1.5 sigma and shown as a blue mesh.

Scheme 1 Reductive Half-Reaction of MR

$$MR_{ox} + NADH \underset{K_{S1-4}}{\overset{^{CT}k_h}{\rightleftharpoons}} (MR_{ox}{\cdot}NADH)^{CT} \xrightarrow{k_{1-4}} MR_{red}{\cdot}NAD^+$$

λ_{max} 464 nm 555 nm colorless

Results and Discussion

Structure of the MR−Coenzyme Complex and the Mechanism of Hydride Transfer. Catalysis by wild-type MR proceeds in two half-reactions, reductive and oxidative, involving three H-transfers by an environmentally coupled quantum tunneling mechanism.[27] The reductive half-reaction involves hydride transfer from the C4 *R*-hydrogen (denoted C4-H) of β-nicotinamide adenine dinucleotide (NADH) to the N5 atom of flavin mononucleotide (FMN). This is observed directly in a rapid mixing stopped-flow instrument and is kinetically resolved from steps involving coenzyme binding and formation of an enzyme−NADH charge-transfer (CT) complex, and the observed kinetic isotope effect (KIE) is essentially the intrinsic KIE (Scheme 1).[7,10,27] In the reductive half-reaction, the 1° KIE for hydride transfer is temperature-dependent[7,27] and the 2° KIE is inflated,[7] consistent with a need for preorganization in an environmentally coupled H-tunneling model.[7] The enzyme requires a promoting motion to move the nicotinamide C4-H sufficiently close to the FMN N5 atom to facilitate tunneling, a notion that is consistent with combined pressure and temperature effects on the 1° KIE and numerical modeling of the reaction parameters in the context of an environmentally coupled framework for H-tunneling.[7,10,27]

1,4,5,6-TetrahydroNADH ($NADH_4$), a nonreactive NADH analogue, is an excellent mimic of the natural coenzyme. We have determined the structure of wild-type MR in complex with $NADH_4$ to inform on the geometry of coenzyme binding and hydride transfer (PDB accession code 2R14). The MR−$NADH_4$ complex was determined at 1.3 Å resolution (Figure 1), and the structure of wild-type MR in complex with $NADH_4$ is essentially identical to that of wild-type MR in the absence of this ligand. Data collection statistics are presented in Supporting

(20) Shi, J.; Palfey, B. A.; Dertouzos, J.; Jensen, K. F.; Gafni, A.; Steel, D. *J. Am. Chem. Soc.* **2004**, *126*, 6914−6922.
(21) Antikainen, N. M.; Smiley, R. D.; Benkovic, S. J.; Hammes, G. G. *Biochemistry* **2005**, *44*, 16835−16843.
(22) Min, W.; English, B. P.; Luo, G. B.; Cherayil, B. J.; Kou, S. C.; Xie, X. S. *Acc. Chem. Res.* **2005**, *38*, 923−931.
(23) Gutfreund, H. *Trends Biochem. Sci.* **1999**, *24*, 457−460.
(24) Warshel, A.; Villa-Freixa, J. *J. Phys. Chem. B* **2003**, *107*, 12370−12371.
(25) Thorpe, I. F.; Brooks, C. L. *J. Phys. Chem. B* **2003**, *107*, 14042−14051.
(26) Bruice, T. C. *Acc. Chem. Res.* **2002**, *35*, 139−148.
(27) Basran, J.; Harris, R. J.; Sutcliffe, M. J.; Scrutton, N. S. *J. Biol. Chem.* **2003**, *278*, 43973−43982.

Information (SI) Table 1. Electron density corresponding to the entire $NADH_4$ molecule was located in the active site, but the temperature factors for $NADH_4$ were higher than those for the protein, suggesting incomplete occupancy even at the high $NADH_4$ concentrations used in the soaks. Three hydrogen bonds are formed between wild-type MR and $NADH_4$; two are made to the carbonyl oxygen of the nicotinamide moiety from residues Asn-189 and His-186 [which are major determinants for the binding of oxidizing substrates such as 2 cyclic enones[28,29]], and the third, from Tyr-356 to the pyrophosphate moiety of the bound nucleotide.

MRCs in the N189A Mutant MR−NADH Complex. We have performed molecular dynamics simulations to investigate the role of the hydrogen bonds from Asn-189 in stabilizing the position of the nicotinamide moiety of NADH. We have focused our studies on wild-type and N189A MR, since a limiting rate of the reductive half-reaction could not be obtained experimentally for the H186A enzyme.[29] The nicotinamide moiety occupies a similar position relative to the isoalloxazine of FMN in wild-type and N189A MR during a significant part of the 10 ns of the dynamics simulations (Figure 2). Additionally in the N189A enzyme the nicotinamide occupies a region of configurational space not accessed in wild-type (configuration 3 in Figure 2A). Analysis of the corresponding structures reveals that configuration 3 can only be accessed when the positional restraint imposed by the hydrogen bond to Asn-189 is removed through mutation (Figure 2). In this configuration, the transferring C4-H atom appears more readily poised for hydride transfer to N5 (at a distance of 3.2 ± 0.4 Å and better overlap with the lone pair) than in configuration 1 (3.5 ± 0.4 Å). This posits that the rate of hydride transfer is faster in N189A enzyme than in wild-type MR, a hypothesis verified by our experimental studies (see below). Additionally, the elevated C4-H−N5 distance in configuration 2 (4.4 ± 0.4 Å) suggests that hydride transfer is far less likely in this configuration. It has been suggested previously[30] that, for formation of a CT complex, the two aromatic rings (i.e., nicotinamide and isoalloxazine) should be largely parallel to each other and in close association; based on our dynamics simulations, wild-type (configuration 1) and N189A (configurations 1 and 3) MR would therefore be expected to produce CT complexes with NADH.

Kinetic Resolution of Putative MRCs in the N189A Enzyme−NADH Complex. Encouraged by our simulation studies, we have conducted detailed stopped-flow studies of FMN reduction by NADH with the N189A MR over extended timescales (200 s) and we find that the absorption change at 466 nm (which monitors FMN reduction) is multiphasic (Figure 3). The reaction transient can be fit to a multiexponential function (eq 1) with at least three rate constants.

$$\Delta A = \sum_{i=1}^{\geq 3} A_i \exp(-k_i t) \qquad (1)$$

where A is the amplitude and k is the rate constant of the ith exponential component, $A\exp(-kt)$, extracted from the stopped-flow trace, and ΔA is the total absorbance change. Using a logarithmic time base and measuring over 50 s, we were able to simultaneously extract rate constants over 3 orders of magnitude between ~200 and 0.2 s^{-1}. Over longer timescales a slower process was also observed, which necessitated data fitting to a fourth exponential. Measuring over >50 s, however, did not allow accurate analysis of the fastest kinetic component. Changes in FMN absorbance did not occur in the dead time of the instrument indicating that faster kinetic components are not lost in the mixing period and no evidence of photobleaching was observed over the extended timescales of these experiments. The amplitudes of the fastest three kinetic components (k_1−k_3) were A_1 ~50%, A_2 ~20−25%, and A_3 ~10−25% of the total absorbance change, with k_4 making a relatively minor contribution to the total absorbance change.

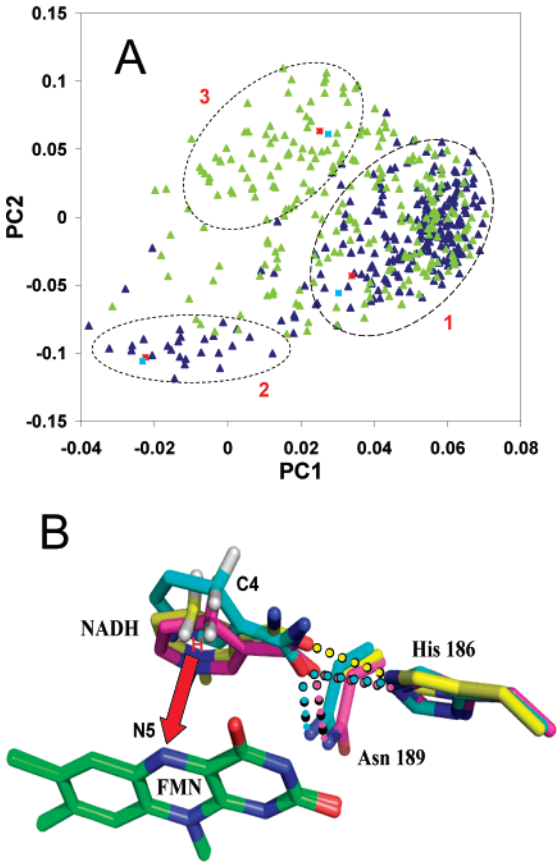

Figure 2. Potential indicators of "tunneling-ready" configurations in wild type and N189A MR enzymes. (A) Principal component analysis from 10 ns molecular dynamics simulations of wild-type (dark blue triangles) and N189A (green triangles) MR. See text and Supporting Information for details. Two major FMN−NADH configurations (labeled 1 and 2) are observed in wild-type, with an additional configuration (3) only observed in the N189A MR simulations. The first two principal components contain 75% of the data. Within each configuration, a structure most similar geometrically to the average structure of that configuration was selected to perform further minimization by first using 50 steps of the steepest descent method followed by applying the conjugate gradient method until the root-mean-square (rms) of the Cartesian elements of the gradient was less than 0.01 kcal/mol/Å. The symbols representing the preminimized structures are colored red, and those corresponding to the minimized structures, in light blue. (B) Relative positions of FMN (isoalloxazine), NADH (nicotinamide), Asn/Ala-189, and His-186 in configurations 1 (carbon atoms in pink), 2 (carbon atoms in cyan), and 3 (carbon atoms in yellow). The transferred hydrogen is shown in red; distances from this hydrogen to N5 are 3.5 ± 0.4, 4.4 ± 0.4, and 3.2 ± 0.4 Å in configurations 1, 2 and 3, respectively. Hydrogen bonds between protein and nicotinamide are depicted as dotted lines. (The isoalloxazine rings of FMN in the three configurations have been overlaid.) Figure 2B is depicted in stereo in SI Figure S1.

(28) Barna, T.; Messiha, H. L.; Petosa, C.; Bruce, N. C.; Scrutton, N. S.; Moody, P. C. E. *J. Biol. Chem.* **2002**, *277*, 30976−30983.
(29) Messiha, H. L.; Bruce, N. C.; Sattelle, B. M.; Sutcliffe, M. J.; Munro, A. W.; Scrutton, N. S. *J. Biol. Chem.* **2005**, *280*, 27103−27110.
(30) Fox, K. M.; Karplus, P. A. *Structure* **1994**, *2*, 1089−1105.

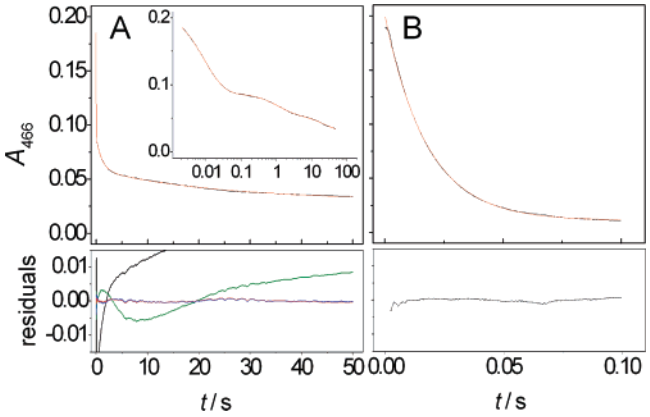

Figure 3. Stopped-flow traces for FMN reduction observed at 466 nm in N189A MR and wild-type enzyme. (A) Reduction of N189A MR; the inset shows the same data on a log scale. Residuals: Black, 1-exponential; green, 2-exponential; blue, 3-exponential; red, 4-exponential fit. (B) Reduction of wild-type MR. The fit shown is that to 1-exponential expression. Conditions: 5 mM NADH in 50 mM potassium dihydrogen orthophosphate, 2 mM 2-mercaptoethanol pH 7.0 at 25 °C.

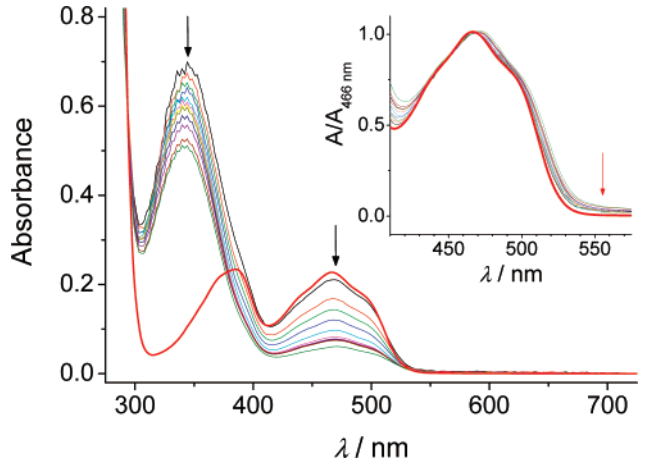

Figure 4. Stopped-flow diode array scans of 20 μM N189A MR following mixing with 100 μM NADH in 50 mM potassium dihydrogen orthophosphate, 2 mM 2-mercaptoethanol pH 7.0 at 5 °C measured between 1.3 ms and 50 s. Arrows indicate the reduction in NADH absorbance at 340 nm and FMN absorbance at 466 nm. Also, shown for reference in bold red is the spectrum of 20 μM oxidized N189A MR. (*Inset*) The spectra normalized to their maximum absorbance showing that the only spectral intermediate is some charge-transfer species that has a slightly red-shifted absorbance at ~470 nm and a weak absorbance at 555 nm (red arrow), which is lost after about 5 s.

We posited that the resolved kinetic phases represent different reactive configurations of the enzyme−NADH complex, consistent with our computational analysis of NADH binding in N189A MR (Figure 1B). The total number of observable reactive configurations is probably indeterminate, with four (i.e., k_1-k_4) being resolved readily using the stopped-flow method. This contrasts with wild-type MR in which FMN reduction occurs in a single kinetic phase.[7] Time dependent absorption changes measured using a photodiode array detector for the reaction of N189A MR with NADH measured over 50 s show only those spectral signatures previously shown to correspond to single-step flavin reduction in the wild-type enzyme (Figure 4).[26] This suggests that the four identified kinetic phases (k_1-k_4) describe the same chemical process, i.e., flavin reduction by hydride transfer.

Analysis of Coenzyme Binding Indicates an Altered Binding Mode in N189A MR. We anticipated that removal of a key interaction between Asn-189 and NADH would weaken the affinity of MR for NADH. Also, our computational analysis suggested there would be an increase in the number of distinct reactive states populated in the mutant enzyme−NADH complex (Figure 2A). Information on both can be gained from stopped-flow studies to obtain the apparent dissociation constant for the enzyme−NADH CT complex and the intensity of the long wavelength absorbance attributed to the CT species that accumulates prior to hydride transfer.[31]

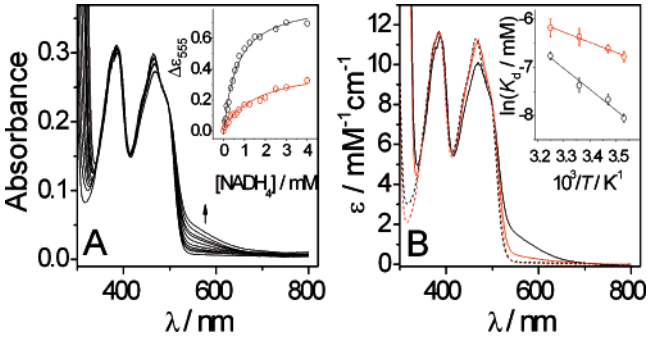

Figure 5. (A) Titration of $NADH_4$ into wild-type MR in 50 mM potassium dihydrogen orthophosphate, 2 mM 2-mercaptoethanol, pH 7.0 at 10 °C. (*Inset*) The absorbance of the CT complex of wild-type (black) and N189A (red) MR at 555 nm as a function of titrated $NADH_4$ at 25 °C. The data are fit to a weak-binding isotherm: $\epsilon = \Delta\epsilon[NADH_4]/(K_d + [NADH_4])$. (B) Absorbance spectra of wild-type (black) and N189A (red) MR in the absence (dotted lines) and presence (solid lines) of saturating $NADH_4$. (*Inset*) The effect of temperature on the apparent dissociation constants of wild-type (black) and N189A (red) MR. The enthalpy (ΔH) and entropy (ΔS) were determined by fitting the data to the van't Hoff equation: $\ln K_a = \Delta S/R - \Delta H/RT$.

We extracted an apparent dissociation constant (K_S) for each of the accessible reactive configurations in N189A MR by analyzing the dependence of the observed rate constant for FMN reduction for each kinetic phase on NADH concentration (SI Figure S2). A value for K_S for the first (K_{S1}) and second (K_{S2}) kinetic phases was determined every 10 °C between 5 and 35 °C by measuring reaction transients at 466 nm. Values for K_S increase linearly with temperature, and fitting to the van't Hoff equation (SI Figure S3) gives values for ΔH and ΔS for the first and second kinetic phases. These data show a stronger temperature dependence on K_{S1} ($\Delta H = 42.8 \pm 5.2$ kJ mol^{-1}) compared to K_{S2} ($\Delta H = 22.0 \pm 4.0$ kJ mol^{-1}). We could not measure accurately a value for K_{S3}, but it appears to be $< \sim 2$ mM based on the data we were able to obtain. The different temperature dependences of K_{S1} and K_{S2} are consistent with different reactive configurations for the enzyme−NADH complex, and their differing K_S values are consistent with the differing amplitudes observed for k_1-k_4.

We have also used the catalytically inactive analogue $NADH_4$ in binding titrations with both wild-type and N189A MR (Figure 5A and B, respectively) across the temperature range 10−35 °C. These data complement the above stopped-flow data and allow a direct comparison of the thermodynamics of coenzyme binding to the wild-type and mutant enzymes. The binding of $NADH_4$ is weaker in N189A MR ($K_d = 1.7 \pm 0.3$ mM) compared with wild-type MR (0.63 ± 0.09 mM) at 25 °C (Figure 5A, *inset*), consistent with there being an altered environment in the active site of the mutant enzyme. The

(31) Craig, D. H.; Moody, P. C. E.; Bruce, N. C.; Scrutton, N. S. *Biochemistry* **1998**, *37*, 7598−7607.

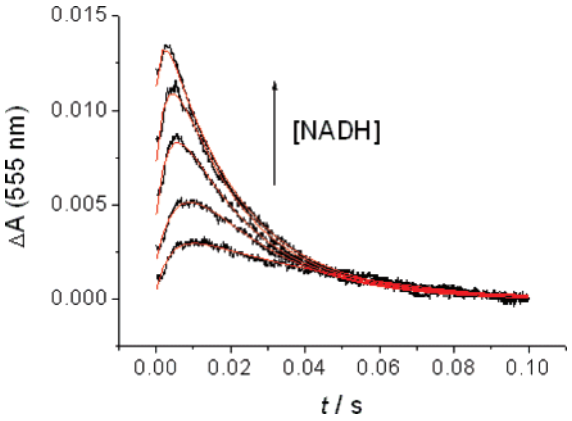

Figure 6. CT complex formation and decay with increasing concentrations of NADH (0.1, 0.2, 0.5, 1, 2, and 5 mM NADH, respectively) and 20 μM N189A MR in 50 mM potassium dihydrogen orthophosphate, 2 mM 2-mercaptoethanol, pH 7.0 at 5 °C.

temperature dependence of the apparent association constant (K_a) is readily calculated from the measured K_d values (Figure 5B, *inset*). Fitting these data for N189A and wild-type MR to the van't Hoff equation describes the thermodynamics of $NADH_4$ binding, giving $\Delta H = -17.1 \pm 1.0$ kJ mol^{-1} (N189A MR) and -35.2 ± 4.0 kJ mol^{-1} (wild-type), and $\Delta S = -4.0 \pm 3.0$ J mol^{-1} K^{-1} (N189A MR) and -58 ± 14 J mol^{-1}K^{-1} (wild-type). Thus, binding is enthalpy-driven, but this is opposed in wild-type MR by a modest negative entropy. This opposing entropic contribution is absent in N189A MR, consistent with more disordered binding of $NADH_4$ to the mutant enzyme. $\Delta G_{binding}$ was estimated from the van't Hoff equation, giving $\Delta\Delta G_{binding}$ (25 °C) $= +3.1 \pm 1.2$ kJ mol^{-1} weaker relative to wild-type MR. These data are consistent with the loss of a hydrogen bond in N189A MR compared to wild-type MR, allowing access to other reactive configurations. We infer in our equilibrium binding titration of N189A MR with $NADH_4$ (Figure 3) we are monitoring specifically the binding of $NADH_4$ in a configuration that mimics the "fastest" N189A MR−NADH reactive configuration (i.e., the first kinetic phase observed at 466 nm). This is supported by the measured extinction coefficient of the N189A MR−$NADH_4$ complex which is significantly less than that measured for the wild-type MR−$NADH_4$ complex (Figure 5). Likewise, the CT species is less intense in stopped-flow reactions of NADH with N189A MR (Figure 6) compared with wild-type MR.[31] We infer that the remaining binding modes detected kinetically (phases 2 to 4) do not contribute significant CT absorbance consistent with the nicotinamide moiety being more distant from and/or positioned less parallel to the FMN isoalloxazine, as also suggested by our computational analysis (Figure 2).

We have also analyzed the kinetics of binding of NADH to N189A MR using stopped-flow methods by following the broad absorbance centered at ~ 555 nm attributed to the MR−NADH CT complex.[31] As with wild-type MR, there is an initial rise in absorbance at 555 nm (CT formation) followed by an absorbance decrease as the CT complex collapses as a result of FMN reduction (Figure 6). We have analyzed the observed rate, $^{CT1}k_{obs}$, of the first kinetic phase (CT formation) as a function of NADH concentration at 5 °C, and fitting these data to the expression $^{CT1}k_{obs} = k_{-b} + k_b[S]$ gives $k_b = (5.4 \pm 0.5) \times 10^5$ M^{-1} s^{-1} and $k_{-b} = 127 \pm 55$ s^{-1} (SI Figure S4A). These values are, within error, the same as those measured previously for wild-type MR [$(4.8 \pm 0.1) \times 10^5$ M^{-1} s^{-1} and 80 ± 6 s^{-1}, respectively].[31]

The decay of the CT band (the second kinetic phase observed at 555 nm) was adequately fit with a single exponential, and the observed rate constant, $^{CT2}k_{obs}$, analyzed as a function of NADH concentration (SI Figure S3B). Data were fit to a single isotherm with a limiting rate constant $^{CT2}k_{lim} = 56.3 \pm 6.1$ s^{-1}. This value is similar to the limiting rate constant (k_{lim1}) for the fastest kinetic phase of FMN reduction measured at 466 nm at the same temperature (66 ± 2 s^{-1}). Additionally, the second kinetic phase at 555 nm saturated with an apparent kinetic $^{CT2}K_S$ of 0.2 ± 0.04 mM, the same, within error, as K_{S1} (0.2 ± 0.02 mM) measured for the first kinetic phase at 466 nm. The amplitude of the absorbance change at 555 nm also saturated as a function of NADH concentration (SI Figure S4B). Given the similar kinetic properties for decay of the CT complex and the first kinetic phase observed at 466 nm (FMN reduction), we infer that the observed CT complex is the same reactant species that defines the first phase of the multiphasic 466 nm transients. We also infer that in our equilibrium binding titration of N189A MR with $NADH_4$ (Figure 5) we are specifically monitoring the binding of $NADH_4$ in a configuration that mimics the "fastest" N189A MR−NADH reactive configuration (i.e., the first kinetic phase observed at 466 nm). This is supported by the measured extinction coefficient of the N189A MR−$NADH_4$ CT complex which is significantly less than that measured for the wild-type MR−$NADH_4$ complex (Figure 5B). Likewise, the CT species is less intense in stopped-flow reactions of NADH with N189A MR (Figure 6) compared with wild-type MR.[31] We infer that the remaining binding modes detected kinetically (phases 2 to 4) do not contribute significant CT absorbance consistent with the nicotinamide moiety being more distant from and/or positioned less parallel to the FMN isoalloxazine, as also suggested by our computational analysis (Figure 2).

Our computational analysis suggests a possible explanation for the existence of multiple phases in N189A MR. The loss of the hydrogen bond from the carbonyl oxygen of the nicotinamide to Asn-189 gives access to a broader range of reactive configurations than in wild-type (configuration 3 and the region between configurations 3 and 2 in Figure 2A). While configuration 3 corresponds to a more optimal reactive configuration than accessible in wild-type (discussed above), the two rings become less parallel when the nicotinamide is located between configurations 3 and 2 — giving a possible explanation for the loss of a CT complex in the additional phases — with C4-H closer to N5 than in (the apparently nonreactive) configuration 2. However, based on our molecular dynamics trajectory of (only) 10 ns, we are unable to assign unique binding modes to phases 2 to 4.

In principle, the observed MRCs can be rationalized in different ways. One could argue that the binding of NADH in multiple conformations at the same active site gives rise to binding conformations that correspond to a different kinetically resolvable exponential component of the absorbance transient reporting on FMN reduction. In this case, one can conceive a number of energetic minima for the $NADH_4$−MR complex, with possible interconversion between them. That we have identified distinct phases of FMN reduction (k_{1-3}), however, argues for slow interconversion of MRCs suggesting trapping of the

coenzyme in local energy minima on binding. Without crystallographic data for the N189A−$NADH_4$ complex we cannot make a definitive statement about the apparent slow interconversion of the MRCs. Our inability to crystallize the mutant complex might reflect heterogeneity in the ensemble population that contributes to the formation of MRCs. Studies at the single molecule level would clearly be informative in evaluating the molecular origin of the observed MRCs.

We have considered an alternative model in which different conformational states of the N189A MR each exhibit different binding modes for the coenzyme, but only one conformational state is competent to catalyze hydride transfer to FMN. We do not favor this model because we observe relatively large primary KIEs for each of the four kinetic phases we access in our stopped-flow studies (see below). Our stopped-flow data indicate relatively slow interconversion of the MRCs, and this would suppress the expression of primary KIEs on those kinetic phases that represent relatively slow conversion of a nonreactive to reactive conformation.

Analysis of 1° and 2° Kinetic Isotope Effects for Each Kinetic Phase in N189A MR. Rate constants, 1° and 2° KIEs, and their temperature dependence, for the chemical (hydride transfer) step in wild-type MR have been reported by us using stopped-flow methods[7] and used to demonstrate an environmentally coupled tunneling reaction.[27] We have extended this stable isotope analysis with the N189A MR to demonstrate that hydride transfer occurs in each kinetic phase observed at 466 nm and to gain insight into tunneling mechanisms. The 1° and 2° KIEs for the hydride transfer reaction for the first three kinetic phases (k_1-k_3) were investigated using (*R*)-[4-^{2}H]-NADH and (*S*)-[4-^{2}H]-NADH, respectively, at coenzyme concentrations that were saturating ($>10 \times K_S$). The temperature dependence of the flavin reduction rate with each coenzyme was measured, and the data were fit using the Eyring equation. Individual rate constants, $\Delta H^{\ddagger}$ and KIEs at each temperature for each of the kinetic phases are given in SI Table 2. The effect of temperature on the corresponding Eyring plots for the N189A enzyme is shown, and corresponding data for the wild-type enzyme are presented for comparison in Figure 7.

The 1° KIEs for the three kinetic phases (KIE_{1-3}) observed in stopped-flow studies at 25 °C are 6.3 ± 0.3, 12 ± 1.7, 4.0 ± 0.5, respectively, and were all found to be temperature-dependent within experimental error and the accessible temperature range. Values of $\Delta\Delta H^{\ddagger} = 4.8 \pm 4.5$ kJ mol^{-1} (KIE_1), 49.5 ± 10.9 kJ mol^{-1} (KIE_2), and 11.6 ± 3.2 kJ mol^{-1} (KIE_3) were obtained. Extracting accurate rate constants for k_2 was more difficult with (*R*)-[4-^{2}H]-NADH because of poorer kinetic resolution of the first and second kinetic phases at certain temperatures. We believe this might be the origin of the larger KIE and observed temperature-dependence for this kinetic phase compared with the first and third kinetic phases.

At 25 °C the magnitudes of the 2° KIE_{1-3} are inflated (i.e., greater than the semiclassical upper limit[32] of 1.13[33]), being 1.3 ± 0.08, 1.23 ± 0.13, and 1.28 ± 0.03, respectively. Inflated 2° KIEs are considered to indicate that H-transfer proceeds by a tunneling mechanism.[32] We have previously observed that for wild-type MR the magnitude of the 2° KIE may reflect the geometry of the "tunneling ready" configuration.[7] The errors for 2° KIE_{1-3} prevents the use of the 2° KIE values to assess any differences in the tunneling ready configuration that one might expect with different MRCs.

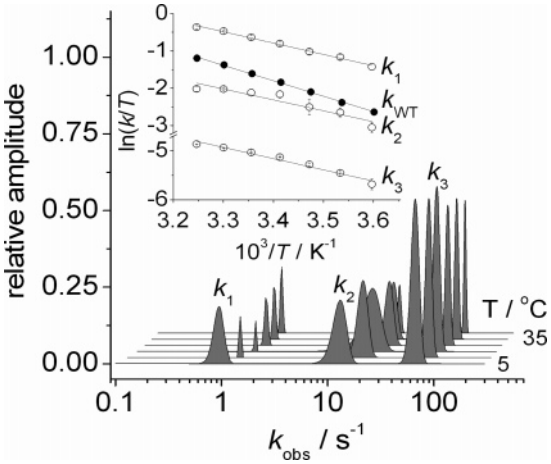

Figure 7. Manifestation of the reactive configurations of N189A MR as a function of temperature. Data collected in 50 mM potassium dihydrogen orthophosphate, 2 mM 2-mercaptoethanol, pH 7.0 using 20 mM NADH and 20 μM N189A. The width of each peak represents the standard error of k_{obs}. The amplitude and k_{obs} for each reactive configuration determined from fitting eq 1 to stopped-flow transients is shown for reactions analyzed between 5 and 35 °C. (*Inset*) The corresponding Eyring plots of the temperature dependence of each accessible reactive configuration and wild-type MR.

The 1° KIEs indicate that hydride transfer occurs in each of the three kinetic phases analyzed at 466 nm. Further, that 1° KIEs > 1 are observed for the three kinetic phases indicates that hydride transfer from NADH to FMN is limiting in each reactive configuration. The inflated 2° KIEs and temperature dependence of the 1° KIEs suggest H-transfer from C4-H occurs by quantum mechanical tunneling in all three characterized reactive configurations. As with wild-type MR,[7,10,27] a role for compressive motion in the enzyme to bring the coenzyme−substrate complex to the tunneling ready configuration is suggested by the temperature dependence of the 1° KIEs. We emphasize the difficulty in rigorously analyzing multiphasic kinetic transients and their temperature-dependence. Thus, while the 2° KIE for the second kinetic phase (KIE_2) is above the semiclassical limit, there is a relatively large error on this value. As regards tunneling, our data for k_2 are arguably equivocal. That said, the key finding is that different reactive configurations can be identified from ensemble stopped-flow measurements of the reductive half-reaction in N189A MR.

MRCs and Implications for the Analysis Enzymatic H-Tunneling. As this and other studies testify, MRCs are more likely to occur following mutagenesis of an enzyme active site.[20,25] Multiple turnover assay methods are unable to detect MRCs, and this has potential implications when using these methods to infer aspects of mechanism (e.g., H-tunneling). Stopped-flow methods have the potential to reveal MRCs when interconversion is slow, as exemplified by our studies with N189A MR, but this is an unusual situation and may prove to be an exception rather than the norm. Experimental detection of MRCs is an important challenge as their existence has major implications for the analysis of reaction data derived from steady-state turnover studies.

It would have been informative to measure steady-state constants for the reaction catalyzed by N189A to illustrate the

(32) Huskey, W. P.; Schowen, R. L. *J. Am. Chem. Soc.* **1983**, *105*, 5704−5706.
(33) Cook, P. F.; Blanchard, J. S.; Cleland, W. W. *Biochemistry* **1980**, *19*, 4853−4858.

impact of forming MRCs when using steady-state turnover methods to address chemical aspects of mechanism. This is not possible with MR as the oxidative half-reaction of both the N189A and wild-type MR enzymes is rate limiting in steady-state turnover,[27] and thus experimental measurement of steady-state rate constants would have little relevance to our analysis of the reductive half-reaction. However, in an attempt to gain some insight we have calculated a hypothetical steady-state (multiple turnover) rate constant (k_{ss}), defined as the rate of overall reaction under multiple turnover conditions when the reductive half-reaction of the catalytic cycle is considered to be rate limiting. Thus, we define k_{ss} as a multiple turnover rate constant in the hypothetical situation where FMN reduction in the N189A enzyme is fully rate limiting and when (i) all binding/release steps in the reductive half-reaction and (ii) all steps in the oxidative half-reaction are faster than flavin reduction. Here k_{ss} is determined from the three limiting rate constants (taken from the analysis of stopped-flow transients at 466 nm) using the following relationship (eq 2):

$$k_{ss} = \sum_i \left(\frac{A_i}{\Delta A} k_i \right) \qquad (2)$$

From this relation, $k_{ss} = 81.5 \pm 12.6\ s^{-1}$ at 25 °C. Comparing this value to those shown in Figure 7 illustrates that the simulated steady-state value does not reflect either of the rate constants k_{1-3} and in this case cannot identify MRCs. We stress that this is a simulated case only, and as a result of the nature of the calculation, the error propagation gives a rather large standard error. That said, the calculation illustrates a failing of steady-state methods in detecting MRCs, and has major implications for the analysis of tunneling regimes in enzymes in those situations where MRCs exist. We emphasize that we do not intend our simulation to exemplify any inadequacy of multiple turnover analysis in general but rather to describe a potential consequence of the observed data for N189A MR.

Tunneling regimes in enzymes are routinely analyzed using steady-state turnover methods and isotopically labeled substrates.[3−5,34] Although kinetic complexity is a concern, intrinsic KIEs can be extracted from kinetic data using established methods.[1] The use of multiple turnover methods has been extended to mutant enzymes to probe the effects of altered active site geometry on tunneling reactions with a number of enzyme systems.[11,35−37] This has led to models of dynamic coupling in H-transfer reactions. Different reactive configurations have been identified primarily from molecular dynamics simulations.[18,19] We suggest that stopped-flow and single molecule studies may therefore be useful tools to augment such steady-state analyses, potentially aiding in describing aspects of kinetic complexity which may arise from mutation of active site residues. The analysis of tunneling regimes for MRCs may prove useful in assessing the contribution, if any, of protein dynamics to hydrogen tunneling. We emphasize, however, that stopped-flow analysis of active-site mutant enzymes will not necessarily identify MRCs. For example, a stopped-flow analysis of several active site mutants of soybean lipoxygenase-1 (SLO-1), an extensively characterized enzyme regarding tunneling mechanisms, has failed to identify MRCs.[38]

With N189A MR, we have shown that MRCs can be identified and analyzed in the same way as single reactive configurations using stopped-flow methods. We have demonstrated a complex interplay of kinetic regimes and reactive configurations in the N189A MR mutant. These data provide a means for describing the occurrence of MRCs mechanistically, building on other stopped-flow,[20] single molecule[20] and computational[18,25] studies. When combined with isotope analysis, stopped-flow studies might prove useful in dissecting apparent artifacts in steady-state studies arising from the presence of MRCs, thus allowing mechanistic details to be discerned.

Experimental Section

All materials were obtained from Sigma-Aldrich (St. Louis, MO), except NADH (which was obtained from Melford Laboratories, Chelsworth, U.K.), [$^2H_6$]ethanol, and [$^2D_1$]glucose (Cambridge Isotope Laboratories, Andover, MA). Wild-type MR and the N189A mutant MR were purified as described previously,[27,31] and the enzyme concentration was determined from absorbance measurements at 466 nm ($\epsilon = 11.3\ mM^{-1}\ cm^{-1}$). As for wild-type MR, the N189A enzyme is stable at room temperature for >12 h as judged by several criteria (retention of full catalytic activity, dynamic light scattering analysis, retention of characteristic FMN absorption spectrum, and the lack of formation of aggregates/precipitation or lack of flavin release from the protein). The preparation of (*R*)-[4-^{2}H]NADH and (*S*)-[4-^{2}H]NADH has been described previously[7] and achieved a similar purity.[7] Isotopic purity was not corrected for in this study[7] due to the negligible effect of minor impurities (<5%) on observed rate constants extracted from stopped-flow data.[7] $NADH_4$ was prepared by passing hydrogen through a solution of NADH containing 10% palladium/carbon catalyst. The reaction was stopped when there was no discernible absorbance at 340 nm and $A_{266}/A_{288} < 1.2$. The coenzyme was then purified as in the case for NADH[7] and stored freeze-dried at −80 °C. Coenzyme solutions were made fresh, and their concentrations were determined by absorbance measurements at 340 nm ($\epsilon = 6.22\ mM^{-1}\ cm^{-1}$; NADH) or 288 nm ($\epsilon = 9.2\ mM^{-1}\ cm^{-1}$; $NADH_4$). All reactions were performed in 50 mM potassium phosphate, 2 mM 2-mercaptoethanol, pH 7.0.

Crystals of $NADH_4$-bound wild-type MR were grown from 45 to 50% saturated ammonium sulfate, 0.1 M HEPES, pH 7.0 using the sitting drop vapor-diffusion method and soaked in 100 mM $NADH_4$. Immediately prior to freezing and X-ray exposure, crystals were transferred to a cryobuffer identical to the mother liquor except for the addition of 20% glycerol. Crystals were then flash-frozen and stored below −170 °C. Data sets were obtained from single crystals mounted in nylon loops and cooled to −170 °C in a gas stream of N_2. Data were collected at the European Synchrotron Radiation Facility (ESRF) at collection station ID142 and processed and reduced using DENZO and SCALEPACK.[39] The crystals were of the same space group as the crystal used for earlier structural determination of MR,[28] so the structure could be solved using difference Fourier analysis. The structure was refined using REFMAC[40] and rebuilt using TURBO.[41]

To prevent oxidase activity of N189A MR, all kinetic studies were performed under strict anaerobic conditions (<5 ppm O_2) within a glovebox environment (Belle Technology) as described previously.[7] Rapid reaction kinetic experiments were performed using an Applied

(34) Wang, L.; Tharp, S.; Selzer, T.; Benkovic, S. J.; Kohen, A. *Biochemistry* **2006**, *45*, 1383−1392.
(35) Bahnson, B. J.; Park, D. H.; Kim, K.; Plapp, B. V.; Klinman, J. P. *Biochemistry* **1993**, *32*, 5503−5507.
(36) Bahnson, B. J.; Colby, T. D.; Chin, J. K.; Goldstein, B. M.; Klinman, J. P. *Proc. Natl. Acad. Sci. U.S.A.* **1997**, *94*, 12797−12802.
(37) Chin, J. K.; Klinman, J. P. *Biochemistry* **2000**, *39*, 1278−1284.
(38) Ruddat, V. C.; Mogul, R.; Chorny, I.; Chen, C.; Perrin, N.; Whitman, S.; Kenyon, V.; Jacobson, M. P.; Bernasconi, C. F.; Holman, T. R. *Biochemistry* **2004**, *43*, 13063−13071.
(39) Otwinowski, Z.; Minor, W. *Methods Enzymol.* **1997**, *276*, 307−326.
(40) Murshudov, G. N.; Vagin, A. A.; Dodson, E. J. *Acta Crystallogra., Sect. D* **1997**, *53*, 240−255.
(41) Rousell, A.; Cambillau, C. *Biographics, Architecture et Fonction des Macromolecules Biologiques (AFMB), Marseilles*; 1992.

Photophysics SX.18MV-R stopped-flow spectrophotometer contained within the glovebox. Spectral changes accompanying flavin reduction were monitored at 466 nm over 20−50 s using a logarithmic time base. For temperature experiments, a saturating coenzyme concentration of 20 mM was used to confer pseudo-first-order reaction kinetics. Individual reaction absorption traces were fit to a multiple exponential expression (eq 1) using Origin 6 software (MicroCal)

Molecular dynamics simulations of wild-type and N189A MR were performed using AMBER8[42] with the AMBER 03 forcefield.[43] The system, comprising 357 residues, FMN and NADH, was solvated in a truncated octahedral water box using the TIP3P model with 10 Å between the edge of the box and the protein. Na^+ ions (18) were added to neutralize the charge of the system. Following equilibration, the production trajectories were collected for 10 ns (SI Figure S4). These trajectories were analyzed using PTRAJ implemented in AMBER8. Principal component analysis was performed on the 2D rmsd matrix of nicotinamide configurations, determined following overlay of the isoalloxazine rings in the different frames, using MATLAB (MathWorks Inc., Natick, MA). For additional details of the computational methods, see legend to SI Figure S4.

(42) Case, D. A.; Cheatham, T. E.; Darden, T.; Gohlke, H.; Luo, R.; Merz, K. M.; Onufriev, A.; Simmerling, C.; Wang, B.; Woods, R. J. *J. Comput. Chem.* **2005**, *26*, 1668−1688.
(43) Duan, Y.; Wu, C.; Chowdhury, S.; Lee, M. C.; Xiong, G. M.; Zhang, W.; Yang, R.; Cieplak, P.; Luo, R.; Lee, T.; Caldwell, J.; Wang, J. M.; Kollman, P. *J. Comput. Chem.* **2003**, *24*, 1999−2012.

Acknowledgment. This work was funded by the UK Biotechnology and Biological Sciences Research Council (BBSRC). N.S.S. is a BBSRC Professorial Research Fellow.

Supporting Information Available: Data collection statistics for the crystal structure of MR bound to $NADH_4$, stereorendered image of Figure 2B, tabulated KIE data, binding data and van't Hoff plots of measured K_S values, plots of CT formation and decay, structural fluctuations over 10 ns trajectory, and computational method details. This material is available free of charge via the Internet at http://pubs.acs.org.

JA074463H